A fluffy sphere-like NiCoCu-carbonate hydroxide based electrocatalyst for the oxygen evolution reaction in pH neutral electrolyte solution

Li Yu,* Xiaocai Ma, Qin Liang

College of Chemistry and Chemical Engineering, Xinyang Normal University, Xinyang 464000, China.

* To whom correspondence should be addressed.

E-mail addresses: yulisunshine@163.com

Materials. All chemicals were purchased from Aladdin (analytical grade) and used without any further purification. The aqueous solutions were prepared using doubledistilled deionized water (Milli-Q grade, Millipore).

Synthesis of $M_2(OH)_2CO_3$. $M_2(OH)_2CO_3$ (M=Ni, Co, and Cu) was synthesized via the reference with some amendment [1-3]. 3 mmol of cobaltous nitrate and 3 g of urea were dispersed in 70 mL of deionized water with stirring for 1 h. Subsequently, the formed mixture was transferred to a reaction vessel and heated to 180 °C for 3 h. After the solution cooled down naturally, the formed powder was obtained by filtration and washed with water and ethanol at least six times. Afterwards, the target product ($Co_2(OH)_2CO_3$) was dried at 45 °C for 12 h. For preparations of $Ni_2(OH)_2CO_3$ and $Cu_2(OH)_2CO_3$, replace cobaltous nitrate with nickel nitrate and copper nitrate, while keeping the rest of the steps unchanged.

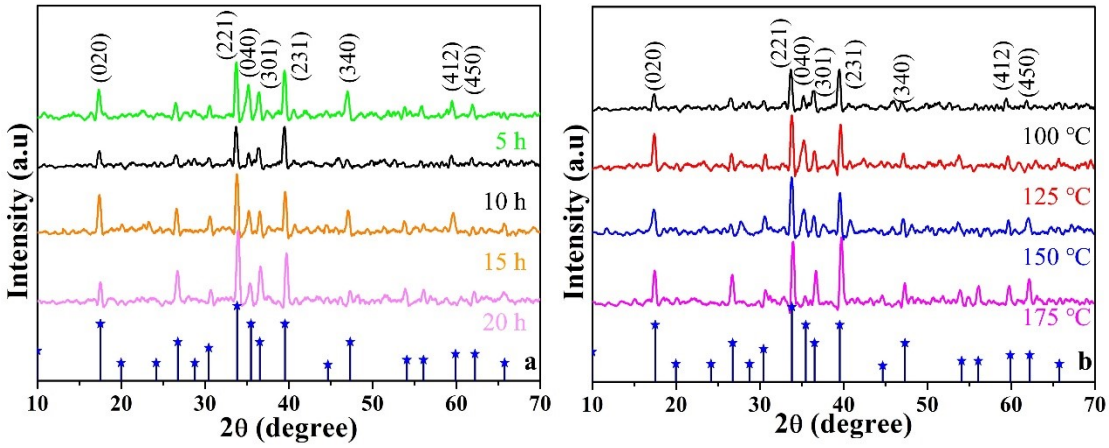

Fig. S1 (a) XRD patterns of $(NiCoCu)(OH)_2(CO_3)$-X-Y prepared at different hydrothermal time: 5 h, 10 h, 15 h, and 20 h at 100 °C. (b) XRD patterns of $(NiCoCu)(OH)_2(CO_3)$-X-Y prepared at different hydrothermal temperatures: 100 °C, 125 °C, 150 °C, and 175 °C for 10 h.

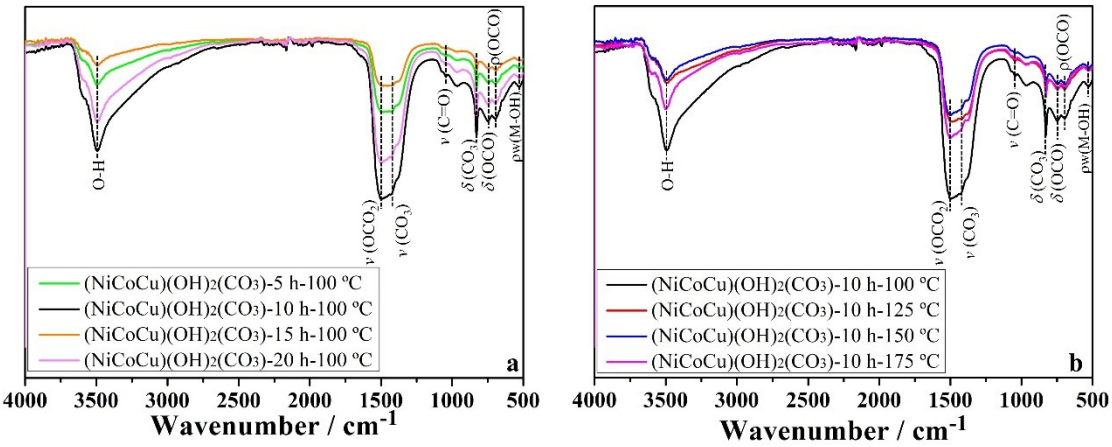

Fig. S2 (a) FT-IR spectra of (NiCoCu)$(OH)_2(CO_3)$-X-Y prepared at different hydrothermal time: 5 h, 10 h, 15 h, and 20 h at 100 °C. (b) FT-IR spectra of (NiCoCu)$(OH)_2(CO_3)$-X-Y prepared at different hydrothermal temperatures: 100 °C, 125 °C, 150 °C, and 175 °C for 10 h.

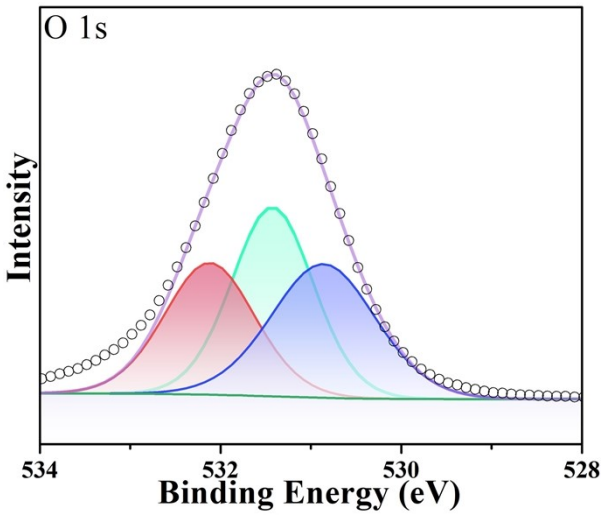

Fig. S3 XPS of (NiCoCu)$(OH)_2(CO_3)$-10 h-100 °C in the energy regions of O 1s.

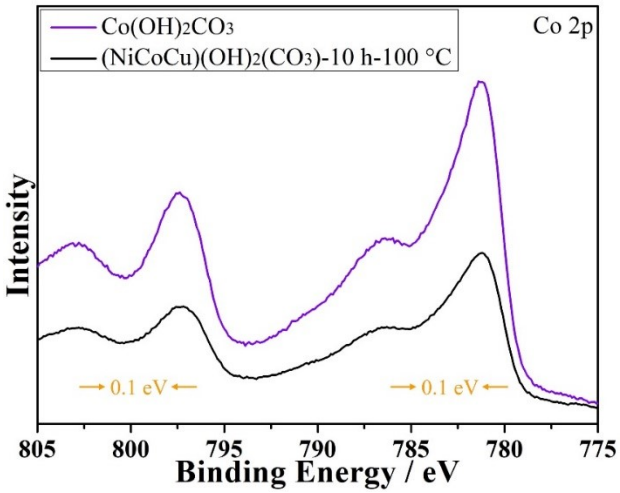

Fig. S4 The high-resolution Co 2p spectra of the $(NiCoCu)(OH)_2(CO_3)$-10 h-100 °C and $Co_2(OH)_2CO_3$.

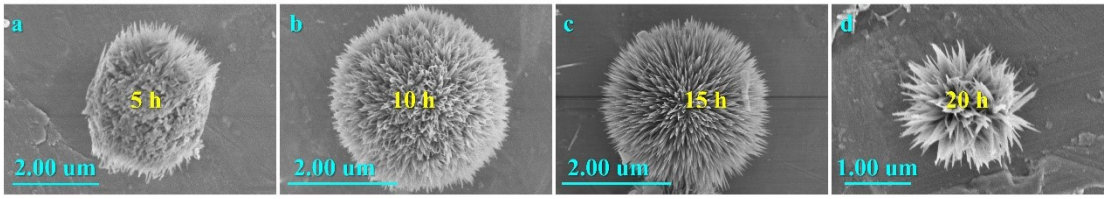

Fig. S5 SEM images of $(NiCoCu)(OH)_2(CO_3)$-X-Y prepared at different hydrothermal time: (a) 5 h, (b) 10 h, (c) 15 h, and (d) 20 h at 100 °C.

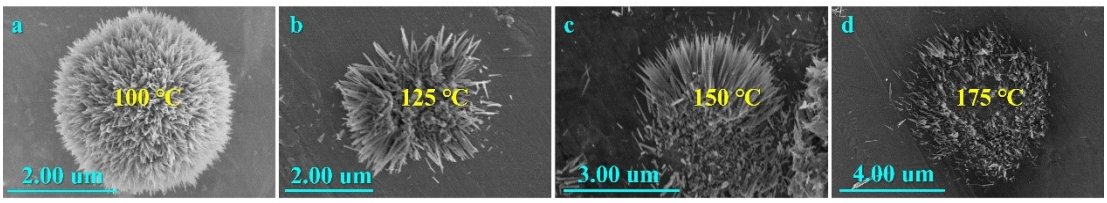

Fig. S6 SEM images of $(NiCoCu)(OH)_2(CO_3)$-X-Y prepared at different hydrothermal temperatures: (a) 100 °C (b) 125 °C, (c) 150 °C, and (d) 175 °C for 10 h.

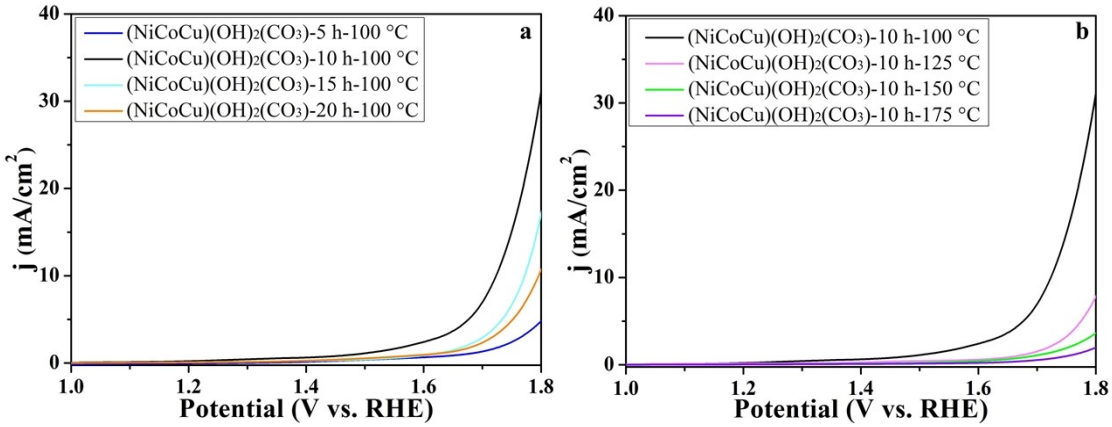

Fig. S7 (a) LSV curves of (NiCoCu)$(OH)_2(CO_3)$-X-Y prepared at different hydrothermal time: 5 h, 10 h, 15 h, and 20 h at 100 °C. (b) LSV curves of (NiCoCu)$(OH)_2(CO_3)$-10 h-100 °C prepared at different hydrothermal temperatures: 100 °C, 125 °C, 150 °C, and 175 °C for 10 h.

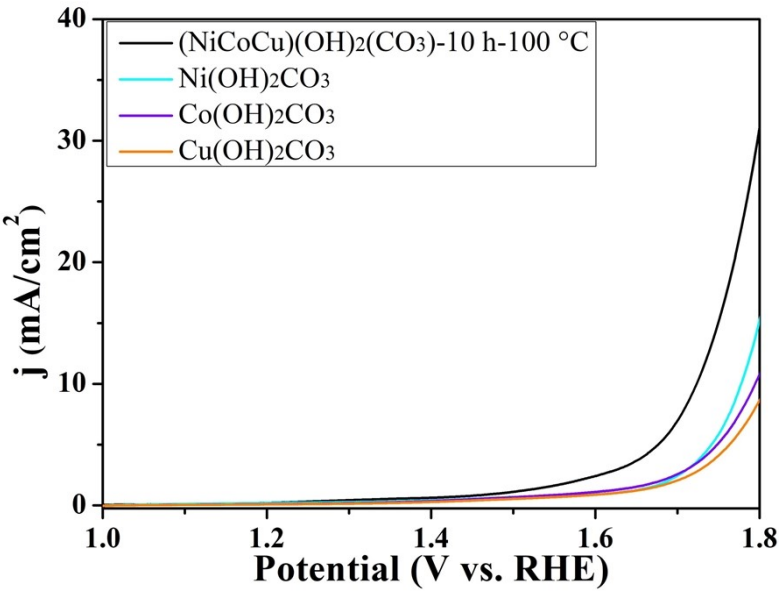

Fig. S8 LSV curves of (NiCoCu)$(OH)_2(CO_3)$-10 h-100 °C, $Ni_2(OH)_2CO_3$, $Co_2(OH)_2CO_3$, and $Cu_2(OH)_2CO_3$. Conditions: Tris-HCl electrolyte (pH = 7.1, 0.2 M), scan rate: 60 mV/s.

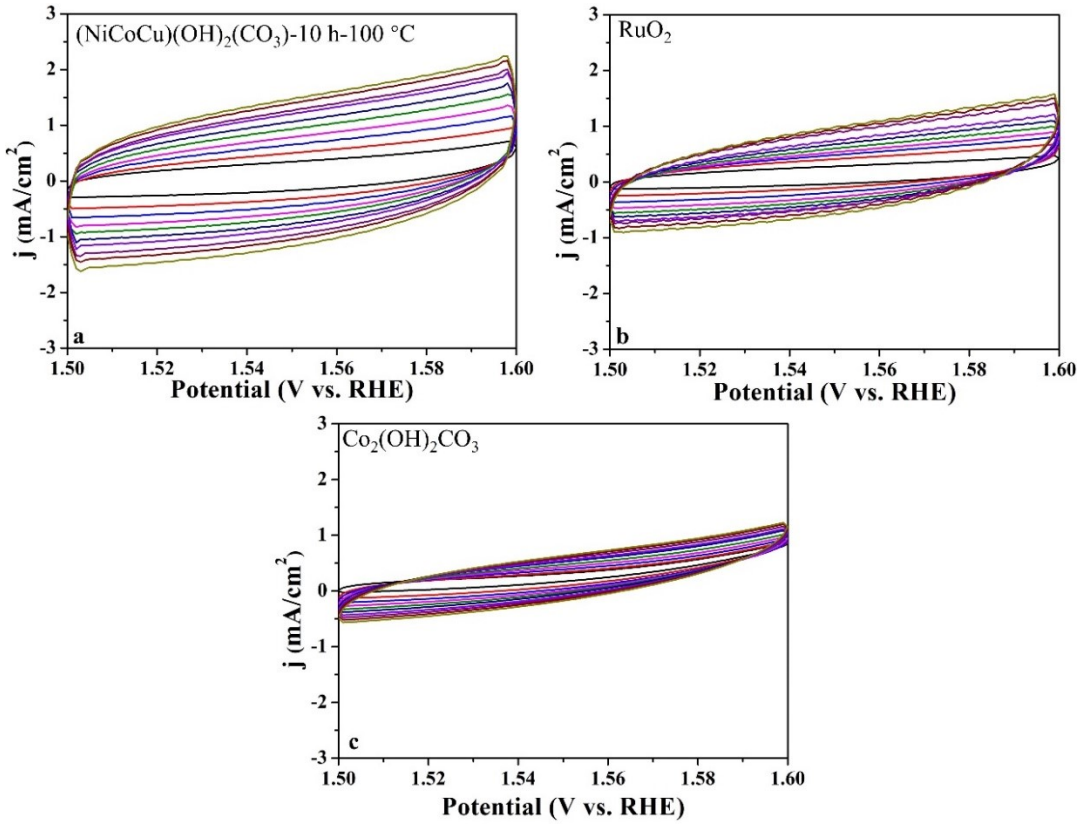

Fig. S9 CV curves measured within the range of 1.5 to 1.6 V *vs.* RHE with scan rate from 20 to 200 mV s^{-1} of (a) $(NiCoCu)(OH)_2(CO_3)$-10 h-100 °C, (b) RuO_2, and (c) $Co_2(OH)_2CO_3$, measured in 0.2 M Tris-HCl buffer solution (pH = 7.1).

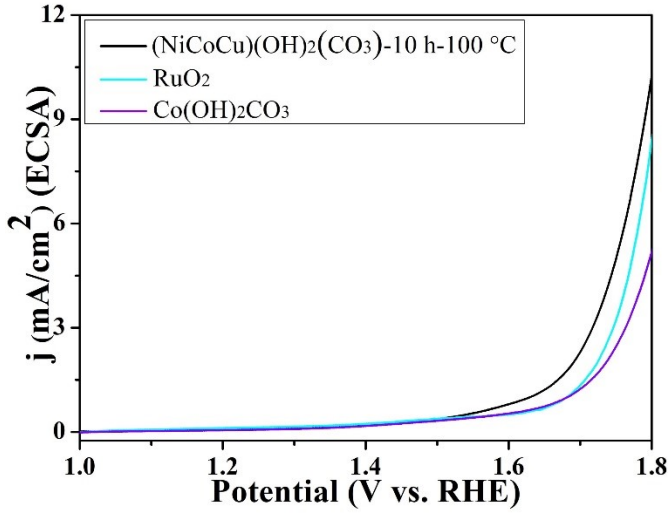

Fig. S10 ECSA-normalized LSV curves of $(NiCoCu)(OH)_2(CO_3)$-10 h-100 °C, RuO_2, and $Co(OH)_2CO_3$ for water oxidation.

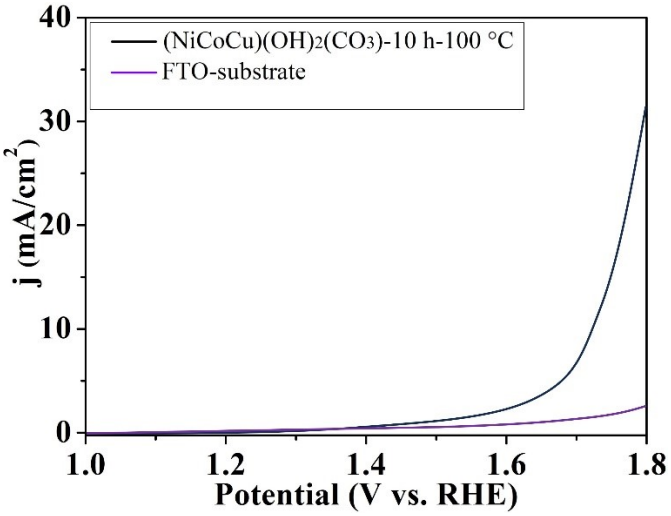

Fig. S11 LSV curves of FTO-substrate and $(NiCoCu)(OH)_2(CO_3)$-10 h-100 °C.

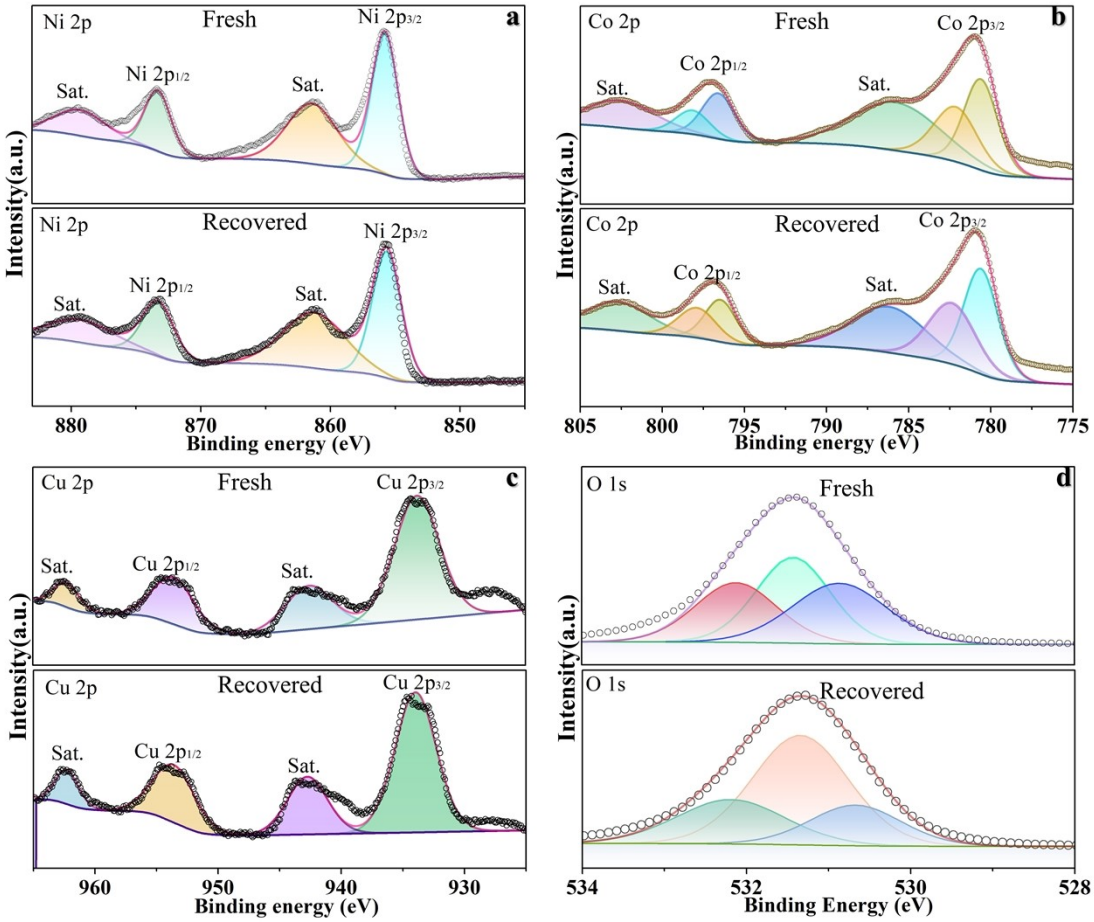

Fig. S12 XPS of $(NiCoCu)(OH)_2(CO_3)$-10 h-100 °C before and after the electrochemical stability experiment in the energy regions of (a) Ni 2p, (b) Co 2p, (c) Cu 2p, and (d) O 1s.

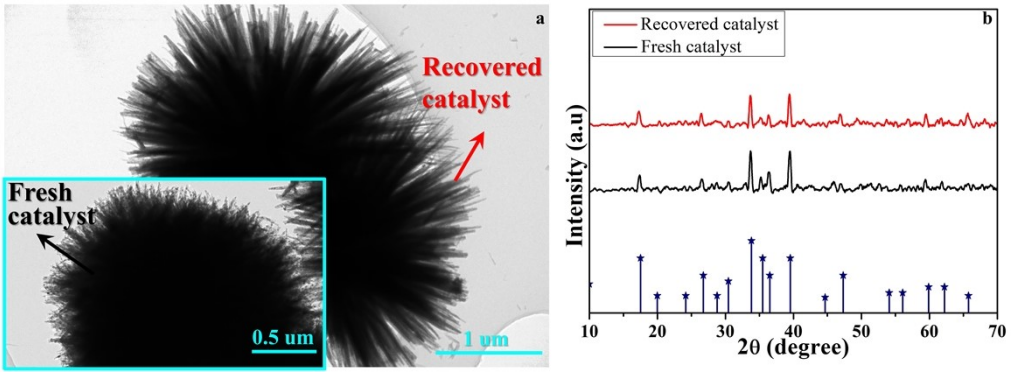

Fig. S13 (a) TEM images and (b) XRD patterns of $(NiCoCu)(OH)_2(CO_3)$-10 h-100 °C before and after chronoamperometric measurement.

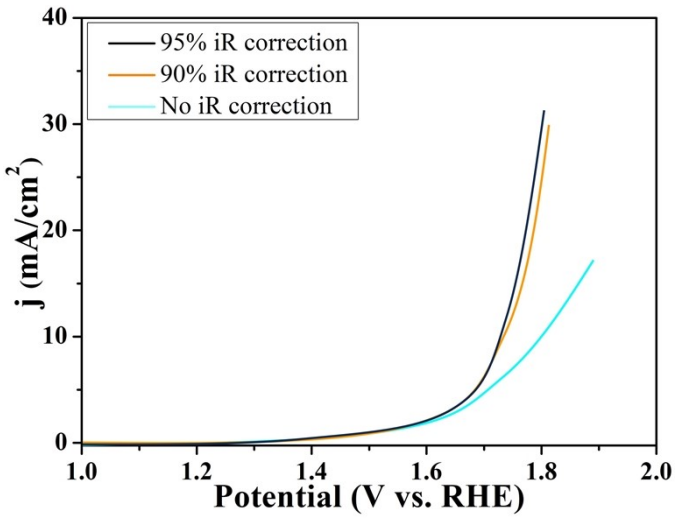

Fig. S14 Polarization curves of $(NiCoCu)(OH)_2(CO_3)$-10 h-100 °C under different iR compensation levels in Tris-HCl electrolyte (pH = 7.1, 0.2 M).

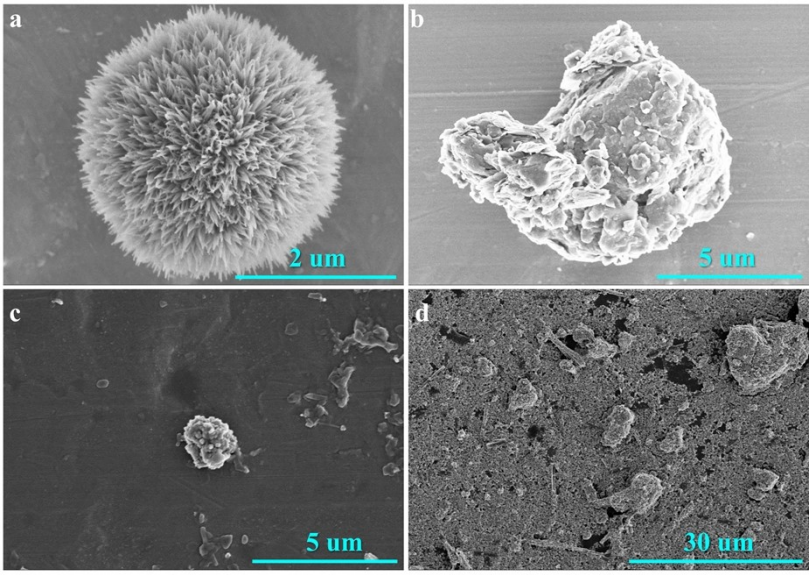

Fig. S15 SEM images of $(NiCoCu)(OH)_2(CO_3)$-10 h-100 °C with varying contents: (a-d) number 1-4 (corresponding to the number in the ICP-AES (Table S4)).

Table S1 BET surface areas and structural parameters of $(NiCoCu)(OH)_2(CO_3)$-X-100 °C

Catalyst	BET surfaces area (m^2/g)[a]	Pore size (nm)[b]	Pore volume (cm^3/g)[c]
$(NiCoCu)(OH)_2(CO_3)$-5 h-100 °C	27.9	1.9	0.1
$(NiCoCu)(OH)_2(CO_3)$-10 h-100 °C	55.3	2.2	0.3
$(NiCoCu)(OH)_2(CO_3)$-15 h-100 °C	46.7	2.8	0.3
$(NiCoCu)(OH)_2(CO_3)$-20 h-100 °C	32.5	3.3	0.4

[a] Surface area obtained from BET measurements.

[b] BJH desorption pore size distribution.

[c] BJH desorption pore volume.

Table S2 BET surface areas and structural parameters of $(NiCoCu)(OH)_2(CO_3)$-10 h-Y

Catalyst	BET surfaces area (m^2/g)[a]	Pore size (nm)[b]	Pore volume (cm^3/g)[c]
$(NiCoCu)(OH)_2(CO_3)$-10 h-100 °C	55.3	2.2	0.3
$(NiCoCu)(OH)_2(CO_3)$-10 h-125 °C	19.7	0.9	0.02
$(NiCoCu)(OH)_2(CO_3)$-10 h-150 °C	13.9	0.5	0.01
$(NiCoCu)(OH)_2(CO_3)$-10 h-175 °C	2.5	0.4	0.01

[a] Surface area obtained from BET measurements.

[b] BJH desorption pore size distribution.

[c] BJH desorption pore volume.

Table S3 ICP-AES date of $(NiCoCu)(OH)_2(CO_3)$-10 h-100 °C with different doped metal content and their OER activity

Number	Sample	Ni (ppm)	Co (ppm)	Cu (ppm)	Overpotential (10 mA/cm^2)
1		2.43	5.27	1.93	490 mV (this work)
2	$(NiCoCu)(OH)_2(CO_3)$	5.33	5.96	1.76	435 mV
3	-10 h-100 ℃	1.86	5.11	5.92	529 mV
4		5.58	5.39	5.10	621 mV

Table S4 EIS fitting results of the components of the circuit shown in Fig. 4d.

Catalyst	R_s (Ω)	CPE (10^{-6})	R_{ct} (Ω)
$(NiCoCu)(OH)_2(CO_3)$-10 h-100 °C	89	0.889	332
RuO_2	96	0.793	624
$Co(OH)_2CO_3$	107	0.975	1433

Table S5 Comparison of some reported materials and this work

Electrocatalyst	Overpotential (mV) @10 mA/cm^2	Tafel mV dec^{-1}	Ref.
Fe-CCHH/NF-30	200 (1.0 M KOH)	50	4
Cu-doped (020)-faceted CCOH	210 (1.0 M KOH)	67	5
t-$Co^{II}Co^{III}$	240 (1.0 M KOH)	79	6
CN-xFe HMs	258 (1.0 M KOH)	48.7	7
$Co_{1.9}Ni_{0.1}(CO_3)(OH)_2$/GP	266 (1.0 M KOH)	44.8	8
5%W-CCH	318 (1.0 M KOH)	65.45	9
CoCH	320 (1.0 M KOH)	38.8	10
CoCH/NF	332 (1.0 M $KHCO_3$)	126	11
$(NiCoCu)(OH)_2(CO_3)$-10 h-100 ℃	490 (pH 7.1, Tris-HCl)	198	This work
CoIr	373 (pH 7, PBS)	117.5	12
C/Co-NPs	390 (pH 7, NaPi)	60	13
$NiFeO_x$/C	400 (pH 7, PBS)	---	14
Co–P–B/rGO	400 (pH 7, PBS)	68	15
$MnS_{0.10}O_{1.90}/MnCo_2S_4$	414 (0.2 M PBS)	78	16
$Ni_{0.33}Co_{0.67}S_2$	420 (pH 7, PBS)	68	17
3D Co–Pi NA/Ti	450 (pH 7.0, PBS)	187	18
CCH@Co-Pi NA/Ti	460 (0.1 M PBS)	284	19
$Fe_{10}Co_{40}Ni_{40}P$	466 (pH 7, PBS)	246	20
$NiCo_2S_4$@N/S-rGO	470 (pH 7, PBS)	---	21
Co–Se–S–O	480 (pH 7, PBS)	---	22
$Co_3(BO_3)_2$@CNT	487 (pH 7, PBS)	63	23
Co_3O_4 QDs	490 (pH 7, PBS)	80	24

Cu_6Co_7/CC	500 (pH 7, PBS)	147	25
$Co_{0.7}Fe_{0.3}P$/CNT	500 (pH 7, PBS)	56	26
CoO/$CoSe_2$ hybrid	510 (pH 6.86, PBS)	137	27
CoP NA/CC	536 (pH 7, PBS)	85	28
δ-MnO_2/FTO	600 (pH 6, Na_2SO_4)	---	29

References

[1] X. Zhou, Y. Zhong, M. Yang, Q. Zhang, J. Wei and Zhen Zhou, *ACS Appl. Mater. Interfaces*, 2015, **7**, 12022.

[2] S. Zhao, Z. Wang, Y. He, H. Jiang, Y. W. Harn, X. Liu, C. Su, H. Jin, Y. Li, S. Wang, Q. Shen and Z. Lin, *Adv. Energy Mater.*, 2019, **9**, 1901093.

[3] L. Zheng, P. Xu, Y. Zhao, J. Peng, P. Yang, X. Shi and H. Zheng, *Electrochim. Acta*, 2022, 412, 140142.

[4] S. Zhang, B. Huang, L. Wang, X. Zhang, H. Zhu, X. Zhu, J. Li, S. Guo and E. Wang, *ACS Appl. Mater. Interfaces*, 2020, **12**, 40220.

[5] X. Y. Liu, H. Bi, L. Li, B. Li, Y. H. Wang, J. Shi, J. Nie, G. F. Huang, W. Hu and W. Q. Huang, *Appl. Phys. Lett.*, 2023, **123**, 093901.

[6] A. Indra, U. Paik and T. Song, *Angew. Chem. Int. Ed.*, 2018, **57**, 1241.

[7] Y. Liu, G. Chen, R Ge, K Pei, C. Song, W. Li, Y. Chen, Y. Zhang, L. Feng and R. Che, *Adv. Funct. Mater.*, 2022, 2200726.

[8] M. Jin, J. Li, J. Gao, W. Liu, J. Han, H. Liu, D. Zhan and L. Lai, *ACS Appl. Energy Mater.*, 2020, **3**, 7335.

[9] M. Jin, J. Li, J. Gao, W. Liu, J. Han, H. Liu, D. Zhan and L. Lai, *J. Colloid Interf. Sci.*, 2021, **587**, 581.

[10] J. Li, X. Li, Y. Luo, Q. Cen, Q. Ye, X. Xu, F. Wang, *Int. J. Hydrogen. Energ.*, 2018, **43**, 9635.

[11] M. Xie, L. Yang, Y. Ji, Z. Wang, X. Ren, Z. Liu, A. M. Asiri, X. Xiong and X. Sun, *Nanoscale*, 2017, **9**, 16612.

[12] Y. Zhang, C. Wu, H. Jiang, Y. Lin, H. Liu, Q. He, S. Chen, T. Duan and Li Song,

Adv. Mater., 2018, **30**, 1707522.

[13] J. Zhu, F. Lambert, C. Policar, F. Mavré and B. Limoges, *J. Mater. Chem. A*, 2015, **3**, 16190.

[14] Y. Qiu, L. Xin and W. Li, *Langmuir,* 2014, **30**, 7893.

[15] P. Li, Z. Jin and D. Xiao, *J. Mater. Chem. A*, 2014, **2**, 18420.

[16] K. Wang, Z. Wang, Y. Liu, J. Liu, Z Cui, X. Zhang, F. Ciucci and Z. Tang, *Chem. Eng. J.*, 2022, **427**, 131966.

[17] Z. Peng, D. Jia, A. M. Al-Enizi, A. A. Elzatahry and G. Zheng, *Adv. Energy Mater.,* 2015, 1402031.

[18] L. Xie, R. Zhang, L. Cui, D. Liu, S. Hao, Y. Ma, G. Du, A. M. Asiri and Xuping Sun, *Angew. Chem. Int. Ed.*, 2016, **55**, 1.

[19] L. Cui, D. Liu, S. Hao, F. Qu, G. Du, J. Liu, A. M. Asirie and X. Sun, *Nanoscale*, 2017, **9**, 3752.

[20] Z. Zhang, J. Hao, W. Yang and J. Tang, *RSC Adv.,* 2016, **6**, 9647.

[21] Q. Liu, J. Jin and J. Zhang, *ACS Appl. Mater. Interfaces*, 2013, **5**, 5002.

[22] Z. M. Luo, J. W. Wang, J. B. Tan, Z. M. Zhang and T. B. Lu, *ACS Appl. Mater. Interfaces*, 2018, **10**, 8231.

[23] E. A. Turhan, S. V. K. Nune, E. Ülker, U. Şahin, Y. Dede, F. Karadas, *Chem.-Eur. J.*, 2018, **24**, 10372.

[24] L. Ma, S. F Hung, L. Zhang, W. Cai, H. B. Yang, H. M. Chen and B. Liu, *Ind. Eng. Chem. Res.*, 2018, **57**, 1441.

[25] M. Wang, W. Zhong, S. Zhang, R. Liu, J. Xing and G Zhang, *J. Mater. Chem. A*, 2018, **6**, 9915.

[26] X. Zhang, X. Zhang, H. Xu, Z. Wu, H. Wang and Y Liang, *Adv. Funct. Mater.,* **2017**, *27*, 1606635.

[27] K. Li, J. Zhang, R. Wu, Y. Yu and B. Zhang, *Adv. Sci.*, 2016, **3**, 1500426.

[28] T. Liu, L. Xie, J. Yang, R. Kong, G. Du, A. M. Asiri, X. Sun and Liang Chen, *ChemElectroChem*, 2017, **4**, 1840.

[29] T. Takashima, K. Hashimoto and R. Nakamura, *J. Am. Chem. Soc.*, 2012, **134**, 1519.